Article

Persulfate Activation Using Biochar from Pomegranate Peel for the Degradation of Antihypertensive Losartan in Water: The Effects of Pyrolysis Temperature, Operational Parameters, and a Continuous Flow Reactor

Alexandra A. Ioannidi [1], Aikaterini Frigana [1], John Vakros [1], Zacharias Frontistis [2] and Dionissios Mantzavinos [1,*]

[1] Department of Chemical Engineering, University of Patras, GR-26504 Patras, Greece; alex.ioannidi@chemeng.upatras.gr (A.A.I.); up1060103@upnet.gr (A.F.); vakros@chemistry.upatras.gr (J.V.)

[2] Department of Chemical Engineering, University of Western Macedonia, GR-50132 Kozani, Greece; zfronistis@uowm.gr

* Correspondence: mantzavinos@chemeng.upatras.gr

Abstract: Biochar derived from pomegranate peel at different pyrolysis temperatures (450, 600, and 850 °C) was synthesized and characterized by BET, XRD, FTIR, and SEM-EDX. Its catalytic efficiency in the degradation of the antihypertensive losartan (LOS) in the presence of sodium persulfate was examined. The biochar pyrolyzed at 850 °C exhibited higher catalytic activity, which was correlated with the greater surface area and higher concentration of minerals on its surface. Interestingly, despite adsorption being favored at alkaline pH, pH 3 showed the highest LOS degradation. LOS decomposition followed pseudo-first-order kinetics. The addition of persulfate significantly increased LOS reduction, while the presence of inorganic and organic water matrix constituents such as sodium chloride, bicarbonate, and humic acid inhibited the oxidation. Experiments conducted with radical scavengers revealed that both hydroxyl and sulfate radicals, as well as singlet oxygen, participated in LOS decomposition, with the former being the dominant species. Using a continuous flow reactor, the system exhibited a satisfactory steady-state performance of 90% LOS removal for 114 h. Afterward, a moderate decrease in performance was observed, which can be attributed to the alteration of the catalyst's surface and mineral dissolution due to acidity.

Keywords: pomegranate peel; pyrolysis temperature; persulfate; pharmaceuticals; continuous flow reactor

1. Introduction

Growing concerns revolve around pharmaceutical contaminants such as antibiotics, anti-inflammatories, antihypertensives, and antidepressants, given their frequent presence in the environment, their ability to contribute to the development of antimicrobial-resistant bacteria, referred to as antibiotics, and their potential toxicity to aquatic organisms [1–4]. Among the various classes of pharmaceutical compounds, the class of antihypertensive drugs is one of the most important, considering that since their discovery, health issues related to heart attacks and strokes caused by high blood pressure have been dramatically reduced [5–8]. Nevertheless, overuse of drugs targeting hypertension has led to their appearance in various aquatic environments, including seawater, rivers, surface water, and hospital wastewater, with concentrations ranging from 0.6 ng/L to 17.7 mg/L [9–16]. Some of the well-known antihypertensive drugs with a high number of prescriptions are losartan (LOS), valsartan, and propranolol [17]. Although LOS is used to prevent heart attacks, strokes, and kidney damage [18,19], it has been reported to be toxic to several organisms, such as *Daphnia magna*, *algae*, *Desmodesmus subspicatus*, and fish [9,20–22]. In addition, LOS has been measured in effluents with concentrations ranging from 0.0197 to

2.760 µg/L [18,23], suggesting the incomplete removal of LOS during biological wastewater treatment [20–22]. Furthermore, in a previous work of our group where Ioannidi et al. [24] studied the degradation of LOS using the heat-activated persulfate (SPS) system, thermally activated persulfate was found to be a particularly energy-intensive process, while some of the identified transformation products of LOS were estimated to be more toxic than the parent compound. Therefore, it is mandatory to explore alternative approaches for the effective degradation of antihypertensive drugs in aqueous environments. Advanced oxidation processes (AOPs) reliant on persulfate activation have gained significant attention in the scientific community for the remediation of persistent micropollutants in aqueous solutions [25,26]; because persulfate is a mild oxidant, it is considerably cheaper than other oxidants such as oxygen peroxide [27], and its activation can be induced through various means, including heat, UV, or even solar irradiation, transition metals, ultrasound, alkaline conditions, carbon materials [28–32], while showing synergistic effects with processes such as photocatalysis [33]. Recently, many researchers have focused on the utilization of biomass residues to produce useful materials [34,35]. In the category of useful products derived from waste biomass, biochar stands out, serving as either an adsorbent material [36,37], a catalyst [38], or a soil improvement agent [39]. The properties of biochar depend on the physicochemical characteristics of the biomass [39,40]. In addition, the characteristics of the obtained materials can be tailored to the variation of the production procedure. Therefore, keeping in mind the perspective of valorization, it is not strange that the number of studies related to biochar has significantly increased in the last decade [41]. A well-known agricultural waste is pomegranate peels, the annual global amount of which is approximately 1.62 million tons [42]; thus, it is considered a potential source to produce biochar. So far, pomegranate peel has been studied as a potential source to produce biochar with a high heating value (23.5 MJ/kg) [43], and to be used as an adsorbent material for crystal violet dye [44]. Only recently, Chen et al. [26] used biochar from pomegranate husk that was pyrolyzed at 500 °C, modified with KOH, $ZnCl_2$, and $KHCO_3$, and continuously pyrolyzed again at 800 °C for peroxymonosulfate (PMS) activation for sulfamethoxazole (SMX) degradation. Chen et al. [26] reported very promising results, but the researchers used PMS as an oxidant, which is more expensive than SPS. Moreover, their work focused on the examination of modified biochar rather than the examination of unmodified biochar, which is more environmentally friendly and does not require additional chemicals. It is also unclear if the slight decrease observed during the catalyst reuse was due to alterations in the catalyst surface. Hadi et al. [45] synthesized magnetic ferric oxide (Fe_3O_4) biochar from pomegranate husk for persulfate activation for the oxidation of 4-Chlorophenol. However, according to the authors, the production of the reactive species was mainly due to the presence of iron. Moreover, Oymak and Şafak [46] synthesized Fe_3O_4 biochar with promising capabilities for the adsorption of sulfadiazine. In addition, Taheri et al. [47] used zinc chloride ($ZnCl_2$) followed by acid treatment to modify biochar from pomegranate husk for 2,4-dichlorophenol adsorption from aqueous solutions.

In this work, biochar derived from pomegranate peels was prepared without any modifications for the first time at three pyrolysis temperatures: 450 °C, 650 °C, and 850 °C. The relevant temperatures were chosen based on the results provided by the work of Chen et al. [26] for the synthesis of pomegranate husk, previous results for the preparation of biochar from other sources [48], and instrumentation limitations.

The biochar was characterized using the Brunauer–Emmett–Teller method (BET) for the determination of the specific surface area (SSA), X-ray diffraction (XRD), Fourier transform infrared (FTIR), scanning electron microscopy (SEM), and energy-dispersive X-ray microanalysis (EDX) techniques. Subsequently, it was investigated for its adsorption and degradation capabilities for LOS, the latter via activated SPS. Additionally, various operational parameters, such as initial SPS and LOS concentrations, were tested, along with the influence of pH, the water matrix, and the degradation pathway, using different scavengers. Since biochars consist of carbon-based material and the stability of these systems remains an open question in the literature, a significant novelty of this work is the

particular emphasis given to determining the catalyst's activity and stability after prolonged treatment times. Therefore, a continuous flow reactor was employed to examine, for the first time, the stability of the pomegranate biochar and to identify factors contributing to the eventual loss of its catalytic activity. This analysis was conducted using XRD, SEM/EDX, and FTIR techniques for both the fresh and the used catalytic material.

2. Results and Discussion

2.1. Biochar Characterization

The specific surface area (SSA) of the materials was measured using the BET method based on data obtained from the adsorption–desorption curves of N_2 at the temperature of liquid nitrogen. All three samples exhibited low SSA values. Specifically, BC450 had a non-detectable SSA, BC650 had a very low SSA of 0.2 m^2/g, and only BC850 had an SSA of 20 m^2/g. As expected, the SSA increases with pyrolysis temperature [49]. Higher pyrolysis temperatures enhance the removal of volatile compounds such as CO, CO_2, and lower hydrocarbons; decompose the raw biomass; and create new pores. These changes result in increased SSA and porosity of the biochar.

The pores of BC850 are primarily located in the macroporosity region, as shown in Figure 1. A small portion of the pores have a mean diameter of 11 nm. The absence of microporosity explains the low SSA of the sample; on the other hand, macroporosity can be beneficial for water movement through biochar in degradation processes, whether in batch or flow oxidation systems.
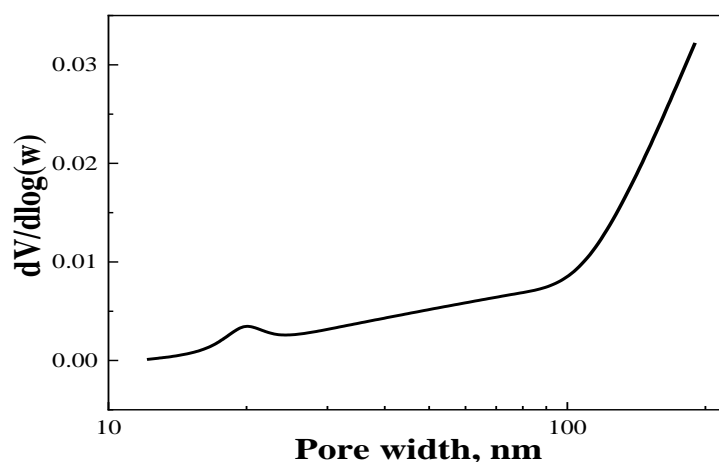
Figure 1. Pore size distribution of the BC850.

The SEM images of the three samples are presented in Figure 2. No significant differences are observable in these images. In all cases, the biochar takes the form of curvy flakes, with only BC850 showing irregular flakes as a result of the higher pyrolysis temperature.

The EDX analysis of the biochars, presented in Table 1, reveals that the main components in all three biochars are carbon (C) and oxygen (O), with respective percentages of 98.3%, 97.9%, and 95.7% for BC450, BC650, and BC850. It is observed that the higher pyrolysis temperature primarily decreases the oxygen content due to the release of a higher amount of volatile species and increases the mineral content in the biochar. These minerals are present in forms such as oxides, hydroxides, or carbonates, indicated by their high basicity. Potassium (K) is the main inorganic component, doubling its content in BC850. Furthermore, it can be deduced that the oxygen content in the carbonaceous phase is lowest in BC850. This can be calculated from the total oxygen content minus the oxygen in minerals. The corrected oxygen contents are 14.9% for BC450, 12.0% for BC650, and 10.1% for BC850. These differences can affect the hydrophilicity of the samples. It should be noted that Na and S were not detected in any of the three biochars.
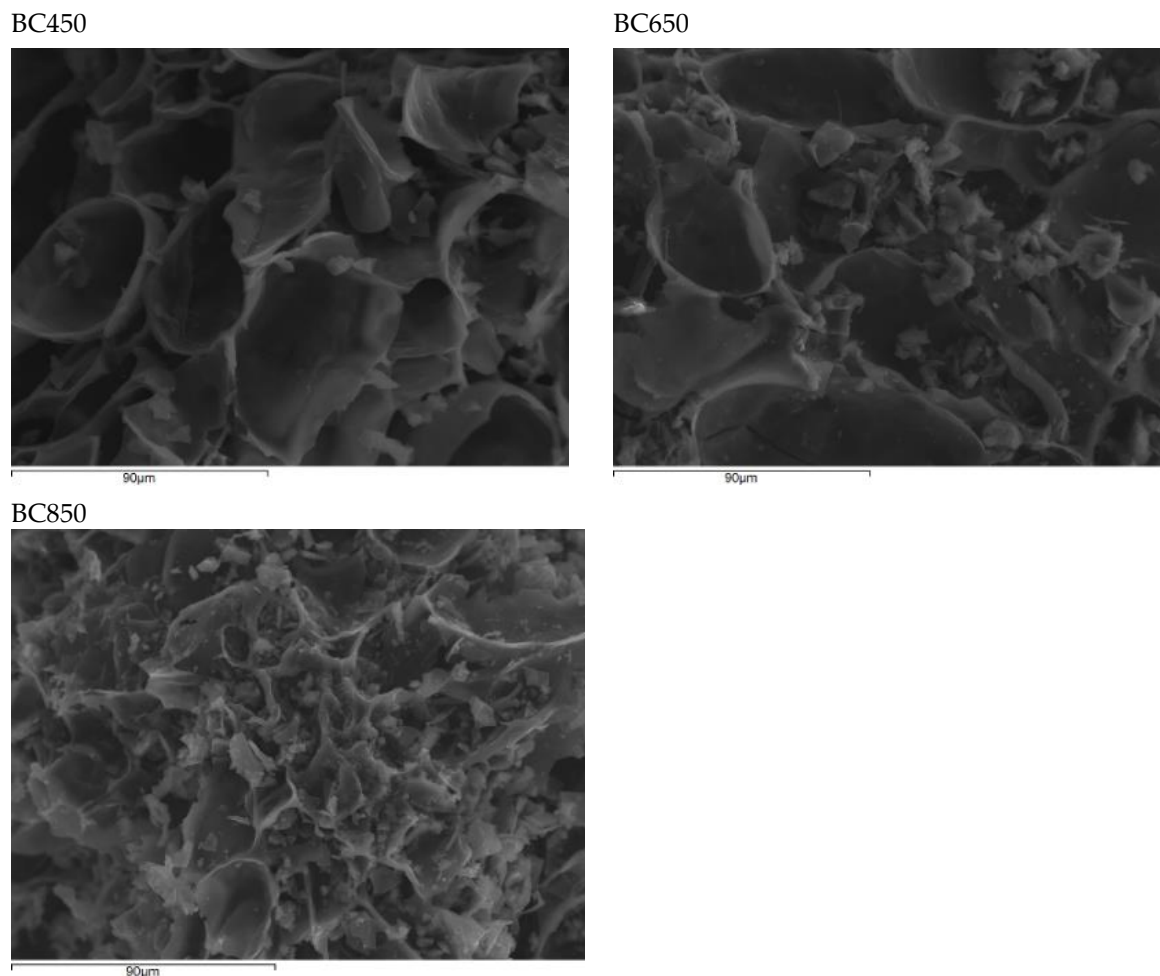
BC450

BC650

BC850

Figure 2. SEM images of the three biochars produced under different pyrolysis temperatures.

Table 1. The % atomic composition of the three biochars determined with EDX.

Element	BC450	BC650	BC850
C	82.5	84.7	83.4
O	15.8	13.2	12.3
Mg	0.1	0.1	0.1
P	0.1	0.1	0.1
Cl	0.1	0.2	0.4
K	1.2	1.5	3.3
Ca	0.2	0.3	0.4

The X-ray diffraction (XRD) peaks of the three biochars are presented in Figure 3.

The three prepared biochars exhibit some intense, sharp peaks in their XRD patterns. These peaks are attributable to the minerals in the biochar, corresponding to various mixed phases of oxides, phosphates, and carbonates. A significant amount of KCl is detectable from the peak at 29.5° [50,51]. Previous reports [52] have indicated that increasing the pyrolysis temperature alters the distribution of minerals in the biochar. Specifically, new peaks were detected, while the intensity of peaks formed at lower temperatures decreased, indicating the decomposition of minerals and the formation of new phases. The broad peaks at approximately 23° and 43° are due to the carbon phase, with the first peak corresponding to the (002) plane of graphitic carbon and the second peak at 43.5° corresponding to sp^2 carbon species (100) [53–55].
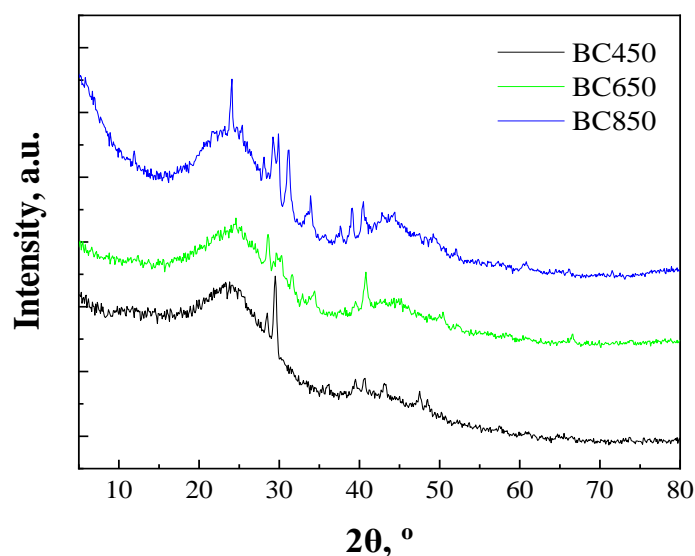
Figure 3. XRD patterns of the three biochar (BC450, BC650, BC850).

The FTIR spectra of the catalysts are presented in Figure 4. It is evident that the three biochars prepared at different pyrolysis temperatures display almost identical peaks, though differences in intensity exist. For instance, the broad peak centered at 3431 cm^{-1} becomes less intense as the pyrolysis temperature increases. This peak represents the –OH bond, and its intensity corresponds with the oxygen content of the samples, as shown in Table 1.
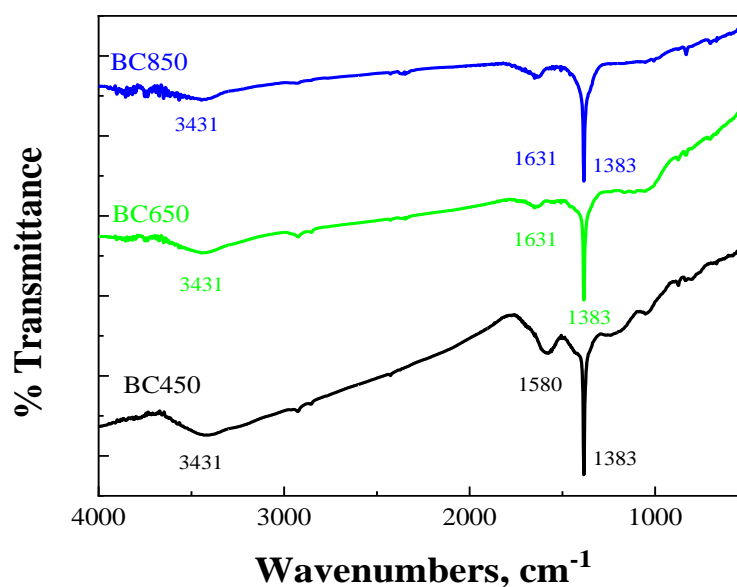

Figure 4. Fourier transform infrared spectra of the studied samples.

The peak at 1580 cm^{-1} is attributed to C=C bonds with conjugation of π electrons [56,57] by functional groups with high electronegativity. This peak shifts to higher wavenumbers with increasing pyrolysis temperatures due to the release of volatile compounds and the graphitization process, which enhances the aromatic character of the biochar [58]. The main peak of the spectrum, located at 1383 cm^{-1}, is associated with carbonate species [59].

2.2. Catalytic Results

2.2.1. Estimation of the Catalytic Activity of Biochars

To investigate the effect of pyrolysis temperatures on the catalytic performance of biochar from pomegranate peel, 500 mg/L of BC450, BC650, and BC850 were used for the degradation of 500 µg/L LOS with 500 mg/L persulfate (SPS) in ultrapure water (UPW) and inherent pH (5.5).

As shown in Figure 5, the degradation rate of LOS increases with the pyrolysis temperature. Removal efficiencies of 65%, 68%, and 95% for LOS were achieved at 180 min for BC450, BC650, and BC850, respectively.
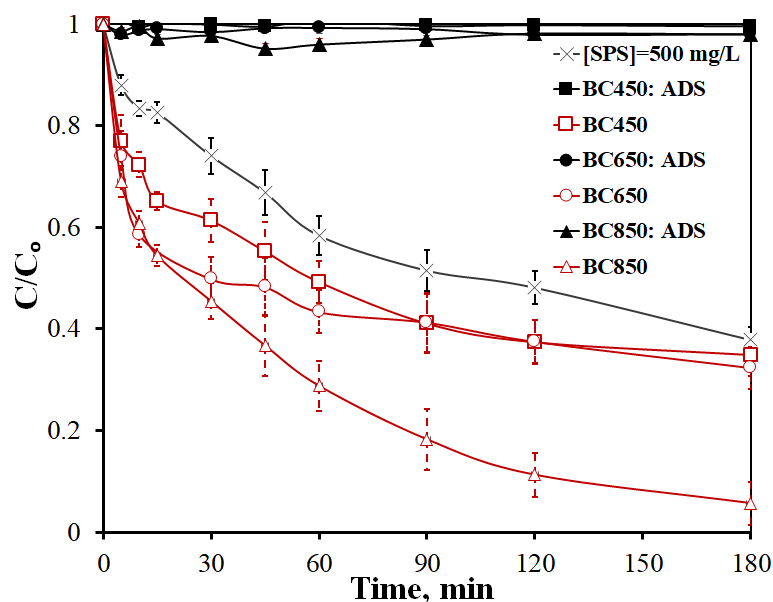
Figure 5. Effect of pyrolysis temperature on biochar catalytic activity under batch operation. Experimental conditions: [Biochar] = 500 mg/L, [SPS] = 500 mg/L, and [LOS] = 500 µg/L in UPW.

This behavior is likely due to the increased specific surface area and the higher percentage of minerals on the surface of the biochar as the pyrolysis temperature increases, as discussed in Section 2.1. Additionally, adsorption experiments were conducted to assess the adsorption capacity of each biochar (Figure 5).

Despite BC850 having a higher SSA compared to BC650 and BC450, the removal of LOS through adsorption at inherent pH was negligible in all cases. Similar results have been reported by Duan et al. [32] and Chen et al. [26], who studied the effect of the pyrolysis temperature to produce soybean straw biochar and pomegranate husk biochar treated with KOH, respectively, to activate persulfate for the degradation of pharmaceuticals. Furthermore, an experiment with 500 mg/L SPS and 500 µg/L LOS was performed, with the results also displayed in Figure 5. It appears that SPS alone is capable of oxidizing a significant portion of LOS, achieving 60% removal after 180 min.

The synergy index, S, is often used in similar catalytic studies to examine if true synergy exists, i.e., whether the simultaneous use of biochar and persulfate exhibits higher efficiency than the sum of the individual biochar (adsorption) and oxidant (persulfate) efficiencies. S can be calculated according to the following equation:

$$S = \frac{k_{BC/SPS}}{k_{BC} + k_{SPS}} \tag{1}$$

where $k_{BC/SPS}$ refers to the apparent kinetic constant for the simultaneous use of biochar and persulfate, k_{BC} refers to the observed kinetic constant in adsorption experiments, and k_{SPS} refers to the apparent kinetic constant in the absence of biochar. Furthermore, true

synergy occurs when S > 1. Interestingly, when applying Equation (1) to the experiments conducted with the various obtained biochars, as depicted in Figure 5, the synergy was calculated to be 1.69, 2.15, and 2.53 for BC450, BC650, and BC850, respectively. These results align with the measured values of persulfate consumption, which decreased from 9% after 10 min of reaction with BC850 to less than 5% for BC450 and BC650, justifying the higher LOS removal observed with BC850.

2.2.2. Effect of Persulfate, Losartan Initial Concentration, pH Solution, and Scavenger Agents

Parameters such as oxidizing agent concentration, persistent pollutant concentration, pH of the solution, and the type of reactive species potentially formed affect the performance of the process and should always be considered.

Figure 6A demonstrates that increasing the SPS concentration enhances the oxidation of LOS. Specifically, LOS removal rates of 62%, 88%, and 99% were achieved in 90 min of reaction with 250, 500, and 750 mg/L SPS, respectively. The apparent rate constant (k_{app}) increased 1.8-fold and 5-fold as the SPS concentration was raised from 250 mg/L to 500 mg/L and to 750 mg/L, respectively.
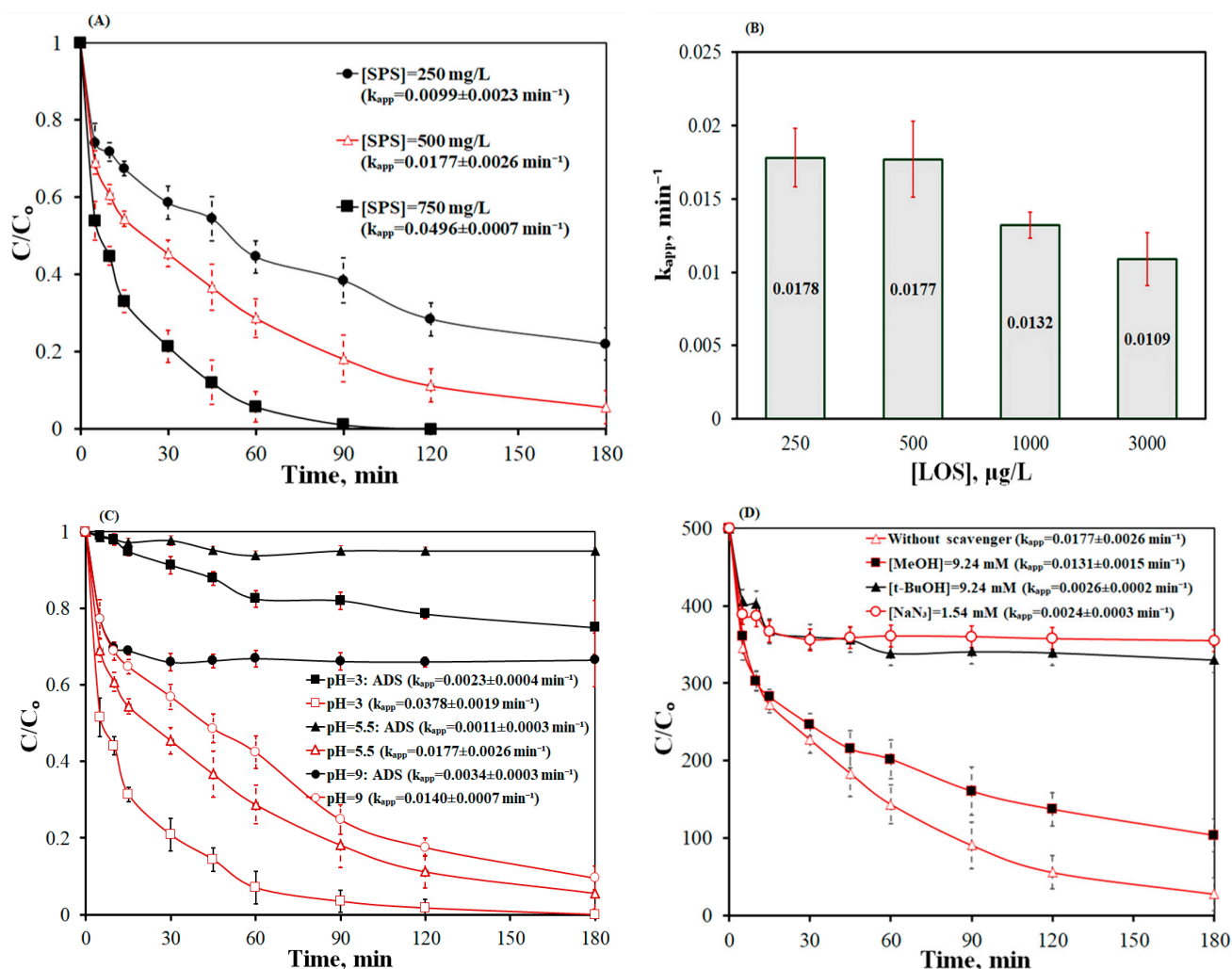
Figure 6. Effect of (**A**) initial concentration of persulfate on 500 μg/L LOS degradation with 500 mg/L BC850, (**B**) initial concentration of LOS on its degradation with 500 mg/L BC850 and 500 mg/L SPS, and (**C**) initial pH solution on 500 μg/L LOS adsorption and degradation with 500 mg/L BC850 and 500 mg/L SPS in UPW. (**D**) Effect of reactive species scavengers on 500 μg/L LOS degradation with 500 mg/L BC850 and 500 mg/L SPS in UPW. Experiments were performed in batch mode of operation.

Although a significant increase in the LOS degradation rate was observed with 750 mg/L of SPS, 500 mg/L of SPS was selected for further investigation based on considerations of (i) potential environmental consequences of sulfate anions in the water, (ii) the process performance, and (iii) the cost of the oxidizing agent [60].

Consequently, the effect of the initial concentration of LOS was tested in the range of 250–3000 μg/L. Figure 6B shows the apparent rate constant (k_{app}) for various initial concentrations of LOS. For LOS concentrations of 250 and 500 μg/L, the degradation rate of LOS follows first-order kinetics. However, concentrations higher than 500 μg/L of LOS resulted in lower k_{app}, indicating that the degradation rate of LOS followed pseudo-first-order kinetics. Specifically, k_{app} decreased from 0.0178 min^{-1} at 250 μg/L LOS to 0.0109 min^{-1} at 3000 μg/L LOS. A similar behavior has been observed in other types of AOPs, such as photocatalysis [61], where for low concentrations of emerging contaminants, k_{app}, remains constant [61–63].

Subsequent experiments were conducted under acidic and basic conditions to study the effect of solution pH on the LOS degradation rate. Figure 6C displays concentration-time profiles at pH values of 3, 5.5, and 9 for both adsorption and degradation of LOS. As shown in Figure 6C, LOS oxidation is more effective in acidic conditions, achieving complete LOS removal within 120 min. However, the degradation rate diminishes with increasing pH; 90% and 82% LOS removal were achieved at pH 5.5 and 9, respectively, after 120 min of treatment, with the k_{app} value decreasing 2.7 times as the pH rose from 3 to 9. In contrast to oxidation, LOS adsorption is favored at pH 9; there is a decrease in LOS adsorption at pH 3, while at the inherent pH, adsorption was almost completely inhibited. This strange behavior can be explained by the fact that LOS contains one acidic and one basic center. The pK values of these groups indicate that there is not a well-separated dissociation of the protonated basic center and the acidic center, leading to equilibria between the positive, neutral, and negative forms of the drug. The cationic form exists at pH values lower than 3.5, while the anionic form can be formed in significant amounts at pH values higher than 5.5. The neutral form of the drug is present in a pH-dependent concentration over the pH range of 1.0 to 6.2, with the maximum concentration located at pH 5. Additionally, the lipophilicity of LOS is maximized in this pH region, showing a peak around pH 5 [64].

The above speciation of LOS suggests that the charge of the species has a significant influence on the adsorption process, and the existence of a charge, either positive or negative, is necessary for adsorption on the biochar surface, despite the biochar's high point of zero charge. This implies that the adsorption is not due to π-π interactions but rather due to electrostatic attractions with the surface hydroxyl groups of the biochar. The limited non-electrostatic interactions are attributed to the low specific surface area of the biochar. On the other hand, the high oxidation of LOS suggests the significant role of the carbonaceous phase in the degradation process. Indeed, the activation of SPS, and thus the oxidation of LOS, is high across all pH ranges. Moreover, the adsorption of SPS on the biochar can influence the total surface charge and, thus, the adsorption of LOS. Therefore, the high oxidation yield in acidic conditions is likely due to the increased adsorption of SPS on the surface of BC850, resulting in the production of more reactive species such as sulfate and hydroxyl radicals [65,66].

To estimate the contributions of sulfate radicals ($SO_4^{\bullet-}$), hydroxyl radicals ($HO^{\bullet}$), and singlet oxygen ($^1O_2$), 9.24 mM of MeOH and t-BuOH, and 1.54 mM NaN_3 were used as scavenger agents, respectively [31,49,67–69]. It should be noted that although NaN_3 is a well-known scavenger for $^1O_2$, it can react with nearly the same kinetic constant with $HO^{\bullet}$ [70,71]. As shown in Figure 6D, the addition of each scavenger reduced the performance of the BC850/SPS process, with both t-BuOH and NaN_3 exhibiting the greatest and equal reduction in performance, where the k_{app} value decreased sevenfold. Conversely, the k_{app} value decreased only 1.35 times with the addition of MeOH. These results indicate that all reactive species studied (i.e., hydroxyl radicals, sulfate radicals, and singlet oxygen) contribute to the oxidation of LOS, with $HO^{\bullet}$ being the dominant species. Similar results

have also been reported by Chen et al. [26], Lykoudi et al. [72], Ho et al. [73], and Avramiotis et al. [49], who studied the activation of persulfates (PMS or SPS) using biochar for the degradation of pharmaceuticals. The high inhibition of degradation observed with the addition of NaN$_3$ also provides evidence that the interactions between biochar, LOS, and SPS are due to the surface C-OH groups. These groups have been found to be active in the oxidation process [74]. Furthermore, the partial oxidation of these groups by SPS leads to the deactivation of the biochar [74].
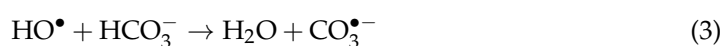
2.2.3. Effect of Water Matrix

Figure 7 illustrates the impact of adding 10 mg/L humic acid (HA) or 250 mg/L of NaNO$_3$, NaCl, and NaHCO$_3$, respectively, as well as the effect of real matrices such as bottled water (BW) and wastewater (WW). Regarding the synthetic water matrices, an inhibition in LOS degradation was observed, except in the presence of NaNO$_3$; the presence of NO$_3^-$ did not significantly affect the LOS degradation rate when using the biochar from pomegranate and SPS. The negligible effect of NO$_3^-$ has also been reported by Ho et al. [73], who used N-doped graphitic biochar from C-phycocyanin to activate persulfate for sulfamethoxazole (SMX) removal.
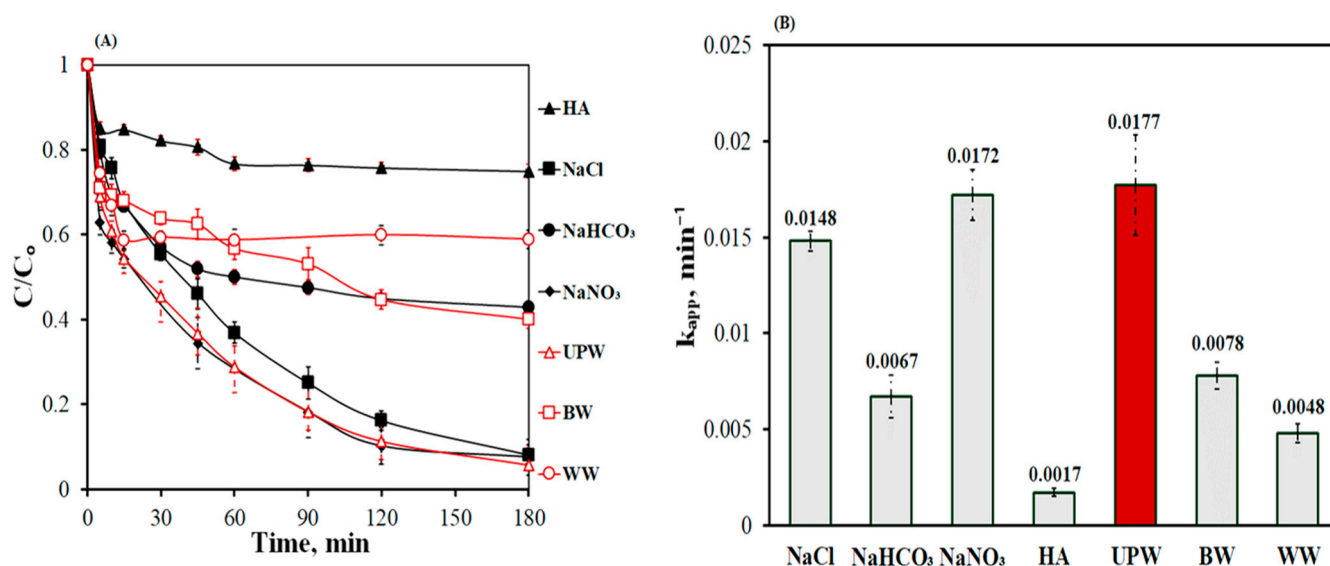
Figure 7. Effect of water matrix on LOS degradation using 500 mg/L BC850 and 500 mg/L SPS. (**A**) concentration-time profiles and (**B**) apparent rate constant k$_{app}$ (R$^2 \geq$ 0.95). Additional experimental conditions: [NaCl] = [NaHCO$_3$] = [NaNO$_3$] = 250 mg/L, [HA] = 10 mg/L, and batch mode of operation.

In this study, LOS removal rates of 89.7%, 90%, 84%, 55%, and 25% were achieved after 120 min of treatment, and the apparent rate constant was calculated to be 0.0177 min^{-1}, 0.0172 min^{-1}, 0.0148 min^{-1}, 0.0067 min^{-1}, and 0.0017 min^{-1} for UPW, NaNO$_3$, NaCl, NaHCO$_3$, and HA, respectively.

Considering the results from the effect of pH and scavengers, it was concluded that the main degradation pathway is radical-based, and LOS degradation decreased in alkaline conditions but not LOS adsorption. The obstructive action of NaCl, NaHCO$_3$, and HA arises from the competition that develops between these substances and LOS for the active centers on the biochar surface and the reactive species generated (SO$_4^{\bullet-}$, HO$^\bullet$) [72]. Cl$^-$ and HCO$_3^-$ react with SO$_4^{\bullet-}$ and HO$^\bullet$, leading to the formation of radicals with lower redox potential, as illustrated by Equations (2)–(6) [67,75–77].

$$SO_4^{\bullet-} + HCO_3^- \rightarrow SO_4^{2-} + HCO_3^\bullet \tag{2}$$

$$HO^\bullet + HCO_3^- \rightarrow H_2O + CO_3^{\bullet-} \tag{3}$$

$$SO_4^{\bullet -} + Cl^- \rightarrow SO_4^{2-} + Cl^\bullet \tag{4}$$

$$Cl^- + HO^\bullet \rightarrow HOCl^{\bullet -} \tag{5}$$

$$Cl^- + HO^\bullet \rightarrow HO^- + Cl^\bullet \tag{6}$$

Similar results have been reported by Chen et al. [26], who studied the activation of PMS for the degradation of sulfamethoxazole (SMX) using KOH-treated biochar from pomegranate. They reported that the presence of both HCO_3^- and Cl^- inhibits SMX decomposition, with Cl^- showing the greatest decrease in SMX oxidation [26].

In the presence of real water matrices, LOS removal of 60% and 40% was achieved after 180 min in BW and WW, respectively. The decrease in performance in real matrices is primarily attributed to the presence of HCO_3^- and organic matter, as detailed in Table 2. This finding is consistent with results reported by Xu et al. [78] and Chen et al. [26]. It can be concluded that when the major degradation pathway is through radicals, which exhibit lower selectivity than the reactive species formed through a non-radical degradation pathway, a decrease in degradation performance is observed in real water matrices. This conclusion is supported by multiple studies. [1,26,29,32,49,56,66,73,78–80].

Table 2. Physicochemical characteristics of the water matrices used in this work.

| Parameter	Wastewater (WW)	Bottled Water (BW)
pH	8.5	7.8
Conductivity (20 °C), [µS/cm]	-	580.2
Total dissolved solids (TDS), [mg/L]	-	380
Total suspended solids (TSS), [mg/L]	22	-
Volatile suspended solids (VSS), [mg/L]	-	-
Total hardness ($CaCO_3$), [mg/L]	-	267
Chemical oxygen demand [mg/L]	48.5	-
Total organic carbon [mg/L]	4.7	-
Chlorides (Cl^-), [mg/L]	262	26.1
Bicarbonates (HCO_3^-), [mg/L]	278	308
Sulfates (SO_4^{2-}) [mg/L]	-	14.7
Phosphates (PO_4^-) [mg/L]	14.98	-
Nitrates (NO_3^-) [mg/L]		12.4
Bromides (Br^-), [mg/L]	165.64	-
Ca^{+2} [mg/L]	112	95.5
Mg^{+2} [mg/L]	-	8.5
K^+ [mg/L]	-	1.02
Na^+ [mg/L]	-	30

It is important to emphasize that the primary objective of this study was to examine the impact of different operating parameters on the BC850/SPS process rather than to enhance system optimization, and no modification was made to the biochar surface.

2.2.4. Continuous Flow Reactor

To examine the stability of BC850, a continuous flow reactor was constructed, as depicted in Scheme 1. Initially, the reactor was supplied solely with 500 µg/L LOS at a flow rate (Q) of 0.36 mL/min until BC850 reached saturation. The residence time was 6.87 min. The required time for BC850 to saturate and for the LOS concentration at the reactor outlet to match that of the feed was 54 h (Figure 8). At 54 h, the feed was changed to feed$_1$ = 1000 mg/L SPS and feed$_2$ = 1000 µg/L LOS with $Q_{in,1}$ and $Q_{in,2}$ at 0.18 mL/min each, achieving a 1:1 dilution and Q_{out} at 0.36 mL/min. As seen in Figure 8, 90% LOS removal was achieved after 3 h of reaction time, and the steady-state performance was maintained for 114 h. Afterward, a small reduction in the degradation yield was noticed. Specifically, a gradual increase in the residual LOS concentration was observed over the next 54 h, reaching 140 µg/L at 168 h.
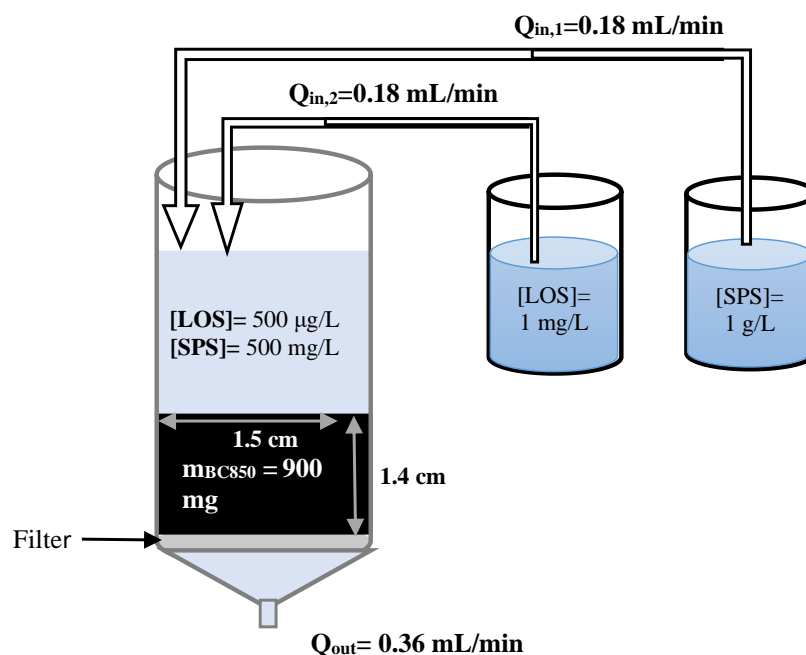
Scheme 1. Illustration of the continuous flow reactor.
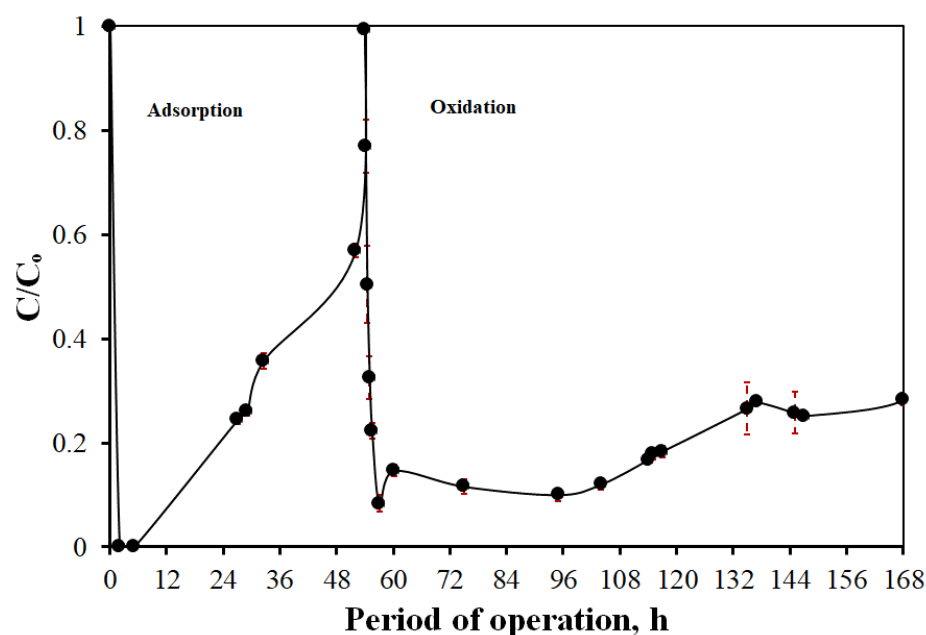
Figure 8. Continuous flow reactor. Experimental conditions: [LOS] = 500 mg/L, [SPS] = 500 mg/L, and m_{BC850} = 900 mg in UPW and inherent pH.

Additionally, the pH of the solution at the outlet of the reactor decreased from 8 at 54 h to 3.08 at 168 h. To further investigate how the surface of BC850 was affected and to explore potential reasons for the decreased degradation performance, the used BC850 was analyzed using XRD, FTIR, SEM, and EDX (Figure 9 and Table 3). As shown in Figure 9A, the XRD pattern of the used sample differed; the sharp peaks were missing, and the two peaks of the carbon species were now more intense and visible, likely due to the oxidation process. The activation of persulfates results in lower pH values, either because the pH was regulated at low values or due to the production of HSO_4^-, a moderately strong acid, as a side product. The acidic environment dissolved the minerals and released them into the solution. These minerals, primarily K, Ca, and Mg ions, which are not harmful to the

environment, have a basic character and readily react with acids. The dissolution of the minerals was also observed in other studies [74,81], where biochar was treated with an acidic solution.
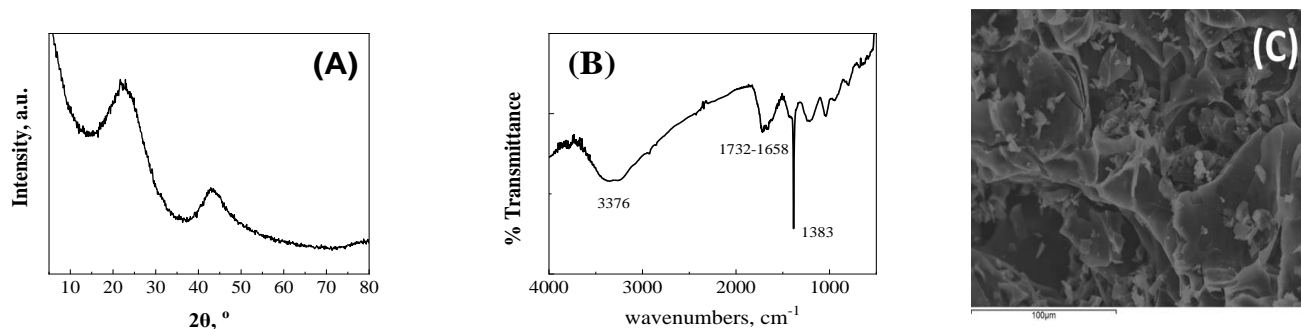
Figure 9. Physiochemical characterization of the used BC850. (**A**) XRD pattern, (**B**) FTIR pattern, (**C**) SEM of BC850 after degradation process.

Table 3. The % atomic composition of used biochar determined with EDX.

Element	BC850
C	90.8
O	7.7
Mg	0.1
P	0.1
Cl	0.1
K	0.5
Ca	0.1
S	0.3
Na	0.3

The FTIR spectrum of the used BC850 (Figure 9B) shows significant differences. The peak at 1383 cm^{-1} is lower, suggesting that the carbonate species were affected by the process, as also indicated by the XRD results. The acidity of the solution interacts with the carbonates, dissolving them and resulting in a lower peak. Another peak at 1732 cm^{-1}, due to C=O species formed on the biochar after SPS oxidation, emerged [82,83]. SPS oxidizes the surface, increasing the C=O content, as proven in previous work using XPS analysis [74], where it was also found that these groups slightly inhibit the catalyst's activity. The broad peak at 3431 cm^{-1} shifted to 3376 cm^{-1} due to the oxidation of C-OH groups.

Furthermore, the SEM image of the used sample (Figure 9C) resembles that of fresh biochar (Figure 2), with the only difference being the reduced presence of minerals. This supports the hypothesis that minerals are dissolved during the oxidation process due to the increased acidity following persulfate activation. HSO_4^-, a moderate acid produced as a side product, lowers the solution pH. The higher acidity and H_3O^+ concentration react with basic minerals like metal oxides, hydroxides, or carbonates, dissolving them. The oxidation process clearly changes the elemental composition of the biochar. As indicated by the values in Tables 1 and 3, the sample is enriched in carbon, while metals, especially K, are significantly reduced, indicating the dissolution of these minerals during oxidation. Interestingly, S and Na, the elements in $Na_2S_2O_8$, are also detected, resulting from the interaction of the biochar surface with persulfate ions. The O content is lower, likely due to the dissolution of minerals rather than the oxidation of C-O groups in the biochar. The dissolution of minerals affects the pH of the interfacial region, thereby altering the speciation of LOS. As a result, the surface becomes less basic, and the LOS speciation shifts towards the neutral form, which is not favored for degradation. On the other hand, the partial oxidation of surface groups hinders the degradation process, as was demonstrated in previous studies [74]. Thus, the decreased yield of the BC850/SPS process is likely due

to the dissolution of minerals present on the BC850 surface and the oxidation of the surface, forming C=O bonds.

3. Materials and Methods

3.1. Materials

Sodium nitrate (NaNO$_3$ ≥ 99.0%, CAS: 7631-99-4), sodium persulfate (SPS ≥ 99.5%), losartan potassium (LOS), humic acid (HA, technical grade), tert-butyl alcohol (*t*-BuOH), sodium azide (NaN$_3$), sodium bicarbonate (NaHCO$_3$), ortho-phosphoric acid (H$_3$PO$_4$ ≥ 85%), and sulfuric acid (H$_2$SO$_4$) were obtained from Sigma-Aldrich (St. Louis, MO, USA). Further details for the above reagents and LOS can be found in the work of Ioannidi et al. [65]. Sodium hydroxide (NaOH, CAS: 1310-73-2) and sodium chloride (NaCl ≥ 99.5%, CAS: 16610-31000) were purchased from Penta (Radiová, Prague, Czechia). Methanol (MeOH, hplc-grade, CAS: 67-56-1) was purchased from Fischer Chemicals (Riesbachstrasse, Zürich, Switzerland). All chemicals were used without any further purification.

Most experiments were performed in ultrapure water (UPW, 18.2 MΩ·cm and pH ≈ 5.5), while commercial BW and secondary effluent from the University of Patras campus wastewater treatment plant (WW) were also used. Details about water matrices can be found in Table 2.

3.2. Preparation of Biochar

A total of 100 g of dry pomegranate peel was washed with ultrapure water (UPW) and dried at 50 °C for 24 h. To examine the effect of pyrolysis temperature, 1 g of pomegranate peel was calcined at 450 °C, 650 °C, and 850 °C for 3 h in N$_2$ atmosphere. The prepared biochars were named BC450, BC50, and B850, respectively.

3.3. Procedure of Degradation Experiments

A typical degradation experiment was carried out in batch mode using 500 μg/L LOS solution at room temperature and atmospheric pressure. The reaction started after the simultaneous dispersion of 500 mg/L biochar and 500 mg/L SPS in 60 mL of aqueous LOS solution without pH adjustment.

During the course of the experiment, 1.2 mL of the reactor contents was withdrawn periodically. The obtained samples were promptly treated by adding 300 μL of methanol and then filtered through a 0.22 μm PVDF syringe filter. Additionally, to estimate the stability of the biochar, a continuous flow reactor (Scheme 1) was used with a flow rate of 0.36 mL/min. In detail, a cylinder reactor from polypropylene was used with inner diameter of 1.5 cm and outer diameter of 1.7 cm. The mass of BC850 was 900 mg, and the height of the cylinder reactor was 12 cm, while the height of the working reactor was 1.4 cm. To achieve the desired flow rates, a Watson-Marlow—205S (Watson-Marlow Fluid Technology Group, Marlow, UK) peristaltic pump was used. During the experiment, samples (1.2 mL) were taken and analyzed using the previously outlined procedure.

3.4. Analytical Methods

The concentration of LOS was monitored by high-performance liquid chromatography (HPLC, waters alliance 2695). Details of the analytical method can be obtained in the work of Ioannidi et al. [24].

For the analysis of bottled water and wastewater, a TOC-LCSH analyzer (Kyoto, Japan) was used to measure the total organic carbon (TOC); the chemical oxygen demand was (COD) measured by the dichromate method using the COD cuvette test—ISO 15705 (0–150 mg/L O$_2$), COD digester (Model LT200, Hach-Lange, Loveland, CO, USA), and Hach Lange DR5000 UV/VIS spectrophotometer [84], while the determinations of ions were achieved using a Dionex ICS-1500 (Sunnyvale, CA, USA) ion chromatography system equipped with an ASRS Ultra II suppressor and an IonPac AS9-HC. The flow rate of the mobile phase was 1 mL/min and consisted of 9 mM carbonate diluted in ultrapure

water [84]. Finally, the determination of bicarbonate was carried out experimentally by titration method using phenolphthalein as indicator [85].

3.5. Biochar Characterization

The produced biochars were characterized with various physicochemical techniques like XRD to identify the possible crystal structures on the biochar, FTIR was used to detect the groups presented on biochar, and the N_2 adsorption—desorption method was used for the determination of specific surface area with BET method. The morphology of the samples was determined using scanning electron microscopy, while the composition of the samples was determined with EDX analysis. Specifically, nitrogen adsorption isotherms were recorded at liquid N_2 temperature using a Micromeritics apparatus (Tristar 3000 porosimeter) (Micromeritics, Norcross, GA, USA). The specific surface area (SSA) of the biochar was determined using the Brunauer–Emmett–Teller (BET) method. X-ray diffraction (XRD) patterns were recorded in a Bruker D8 Advance diffractometer (Bruker, Billerica, MA, USA) equipped with a nickel-filtered CuKa (1.5418 Å) radiation source. The step size and the time per step were, respectively, fixed at 0.02° and 0.5 s in the range of $10° \leq 2\,\theta \leq 80°$. Fourier transform infrared (FTIR) spectroscopy was performed using a Perkin Elmer Spectrum RX FTIR system (Perkin Elmer, Waltham, MA, USA). The measurement range was 4000–400 cm^{-1}. Biochar (about 1%) and KBr were sieved and pressured to produce a homogeneous disk. The morphology of the biochar was examined using a scanning electron microscope (SEM) (JEOL, JSM-6300) (JEOL, Tokyo, Japan) operating at 20 kV, equipped with an X-ray energy-dispersive spectrometer (EDX) (Oxford, UK). Surface analysis measurements were performed in a UHV chamber (P~5 × 10^{-10} mbar) equipped with a SPECS Phoibos 100-1D-DLD hemispherical electron analyzer (SPECS Surface Nano Analysis GmbH, Berlin, Germany) and a non-monochromatized dual-anode Mg/Al X-ray source. Analytical details about the experimental procedure for these techniques can be found in Ntoufra et al. [74], Giannakopoulos et al. [86], and Avramiotis et al. [87].

3.6. Data Analysis

LOS oxidation follows a pseudo-first-order kinetic rate with $R^2 > 0.95$ in every instance. The apparent rate constants (k_{app}, min^{-1}) were computed using Equation (7):

$$\text{rate} = -\frac{dC}{dt} = k_{app}C \rightarrow \ln\left(\frac{C}{C_o}\right) = -k_{app}t \tag{7}$$

where C_o, and C refer to LOS quantity at time zero and t, respectively.

Residence time was calculated using Equation (8) [88].

$$t = \frac{V}{Q} = \frac{\pi d^2 L}{4Q} \tag{8}$$

4. Conclusions

This work investigated the synthesis and characterization of biochar from pomegranate peel at different pyrolysis temperatures. The as-prepared biochars, without any modifications, were used to (i) remove LOS by adsorption and (ii) oxidize LOS by the reactive species formed through the activation of SPS. Particular emphasis was given to examining the catalyst's stability and the performance of the system under continuous flow. In summary, the main conclusions of the study are as follows:

- Among the different temperatures examined (450, 650, 850 °C), the highest (850 °C) exhibited greater catalytic efficiency due to the enhanced (i) surface area and (ii) presence of minerals on its surface;
- The oxidation followed pseudo-first-order kinetics, and the apparent kinetic constant decreased with increasing concentration;
- As expected, the reaction rate was elevated with increased SPS loading;

- Despite a basic pH being favorable for adsorption, the catalytic activity was enhanced in acidic conditions due to the enhanced role of the SPS in the oxidation process;
- Both hydroxyl and sulfate radicals, as well as singlet oxygen, participated in the LOS destruction, with the former serving as the dominant species;
- The system's efficiency was reduced in the presence of carbonates, chlorides, and humic acid due to the scavenging of the reactive species, indicating a radical mechanism, but efficiency remained unchanged in the presence of nitrates;
- The system exhibited high stability using a continuous flow reactor, retaining a 90% LOS removal for more than 114 h. The moderate drop in system efficiency observed over longer treatment times was attributed to the alteration of the catalyst's surface and mineral dissolution due to acidity.

References

1. Zhang, R.; Li, Y.; Wang, Z.; Tong, Y.; Sun, P. Biochar-activated peroxydisulfate as an effective process to eliminate pharmaceutical and metabolite in hydrolyzed urine. *Water Res.* **2020**, *177*, 115809. [CrossRef]
2. Priya, A.K.; Gnanasekaran, L.; Rajendran, S.; Qin, J.; Vasseghian, Y. Occurrences and removal of pharmaceutical and personal care products from aquatic systems using advanced treatment—A review. *Environ. Res.* **2022**, *204*, 112298. [CrossRef] [PubMed]
3. Jiang, J.-Q.; Zhou, Z.; Sharma, V.K. Occurrence, transportation, monitoring and treatment of emerging micro-pollutants in wastewater—A review from global views. *Microchem. J.* **2013**, *110*, 292–300. [CrossRef]
4. Busch, W.; Schmidt, S.; Kühne, R.; Schulze, T.; Krauss, M.; Altenburger, R. Micropollutants in European rivers: A mode of action survey to support the development of effect-based tools for water monitoring: Micropollutants in European rivers: A mode-of-action. *Environ. Toxicol. Chem.* **2016**, *35*, 1887–1899. [CrossRef] [PubMed]
5. Kane, S.P. Valsartan, ClinCalc DrugStats Database, Version 2022.08. ClinCalc. Available online: https://clincalc.com/DrugStats/Drugs/Valsartan (accessed on 29 July 2023).
6. Statista: Number of Losartan Potassium Prescriptions in the U.S. from 2004 to 2020 (in Million). Available online: https://www.statista.com/statistics/781681/losartan-potassium-prescriptions-number-in-the-us/ (accessed on 29 July 2023).
7. Centers for Disease Control and Prevention. Hypertension Cascade: Hypertension Prevalence, Treatment and Control Estimates Among U.S. Adults Aged 18 Years and Older Applying the Criteria from the American College of Cardiology and American Heart Association's 2017 Hypertension Guideline—NHANES 2017–2020. Atlanta, GA: 12 May 2023. Available online: https://www.cdc.gov/bloodpressure/facts.htm#:~:text=This%20includes%2037%20million%20U.S.%20adults.&text=About%2034%20million%20adults%20who,140/90%20mmHg%20or%20higher (accessed on 6 July 2023).
8. Rouette, J.; McDonald, E.G.; Schuster, T.; Brophy, J.M.; Azoulay, L. Treatment and prescribing trends of antihypertensive drugs in 2.7 million UK primary care patients over 31 years: A population-based cohort study. *BMJ Open* **2022**, *12*, e057510. [CrossRef] [PubMed]
9. Cortez, F.S.; Souza, L.S.; Guimarães, L.L.; Almeida, J.E.; Pusceddu, F.H.; Maranho, L.A.; Mota, L.G.; Nobre, C.R.; Moreno, B.B.; Abessa, D.M.S.; et al. Ecotoxicological effects of losartan on the brown mussel Perna perna and its occurrence in seawater from Santos Bay (Brazil). *Sci. Total Environ.* **2018**, *637–638*, 1363–1371. [CrossRef] [PubMed]
10. Mandaric, L.; Diamantini, E.; Stella, E.; Cano-Paoli, K.; Valle-Sistac, J.; Molins- Delgado, D.; Bellin, A.; Chiogna, G.; Majone, B.; Diaz-Cruz, M.S.; et al. Contamination sources and distribution patterns of pharmaceuticals and personal care products in Alpine rivers strongly affected by tourism. *Sci. Total Environ.* **2017**, *590–591*, 484–494. [CrossRef] [PubMed]
11. Nuel, M.; Laurent, J.; Bois, P.; Heintz, D.; Wanko, A. Seasonal and ageing effect on the behaviour of 86 drugs in a full-scale surface treatment wetland: Removal efficiencies and distribution in plants and sediments. *Sci. Total Environ.* **2018**, *615*, 1099–1109. [CrossRef]

12. Ashfaq, M.; Li, Y.; Wang, Y.; Chen, W.; Wang, H.; Chen, X.; Wu, W.; Huang, Z.; Yu, C.-P.; Sun, Q. Occurrence, fate, and mass balance of different classes of pharmaceuticals and personal care products in an anaerobic-anoxic-oxic wastewater treatment plant in Xiamen, China. *Water Res.* **2017**, *123*, 655–667. [CrossRef]

13. Botero-Coy, A.M.; Martínez-Pachon, D.; Boix, C.; Rincon, R.J.; Castillo, N.; Arias- Marín, L.P.; Manrique-Losada, L.; Torres-Palma, R.; Moncayo-Lasso, A.; Hernandez, F. 'An investigation into the occurrence and removal of pharmaceuticals in Colombian wastewater'. *Sci. Total Environ.* **2018**, *642*, 842–853. [CrossRef]

14. Casado, J.; Rodríguez, I.; Ramil, M.; Cela, R. Selective determination of antimycotic drugs in environmental water samples by mixed-mode solid-phase extraction and liquid chromatography quadrupole time-of-flight mass spectrometry. *J. Chromatogr. A* **2014**, *1339*, 42–49. [CrossRef]

15. Wang, J.; Wang, S. Activation of persulfate (PS) and peroxymonosulfate (PMS) and application for the degradation of emerging contaminants. *Chem. Eng. J.* **2018**, *334*, 1502–1517. [CrossRef]

16. Serna-Galvis, E.A.; Isaza-Pineda, L.; Moncayo-Lasso, A.; Hernández, F.; Ibáñez, M.; Torres-Palma, R.A. Comparative degradation of two highly consumed antihypertensives in water by sonochemical process. Determination of the reaction zone, primary degradation products and theoretical calculations on the oxidative process. *Ultrason. Sonochem.* **2019**, *58*, 104635. [CrossRef] [PubMed]

17. Kalinić, D.; Škrbić, R.; Vulić, D.; Stojaković, N.; Stoisavljević-Šatara, S.; Stojiljković, M.P.; Marković-Peković, V.; Golić Jelić, A.; Pilipović-Broćeta, N.; Wong, N.D.; et al. Trends in Antihypertensive Medicine Utilization in the Republic of Srpska, Bosnia and Herzegovina: An Eleven-Year Follow-Up. *Front. Pharmacol.* **2022**, *13*, 889047. [CrossRef] [PubMed]

18. Kaur, B.; Dulova, N. UV-assisted chemical oxidation of antihypertensive losartan in water. *J. Environ. Manag.* **2020**, *261*, 110170. [CrossRef] [PubMed]

19. Israili, Z.H. Clinical pharmacokinetics of angiotensin II (AT 1) receptor blockers in hypertension. *J. Hum. Hypertens.* **2000**, *14*, S73–S87. [CrossRef] [PubMed]

20. Bayer, A.; Asner, R.; Schüssler, W.; Kopf, W.; Weiß, K.; Sengl, M.; Letzel, M. Behavior of sartans (antihypertensive drugs) in wastewater treatment plants, their occurrence and risk for the aquatic environment. *Environ. Sci. Pollut. Res. Int.* **2014**, *21*, 10830–10839. [CrossRef] [PubMed]

21. Osorio, V.; Larrañaga, A.; Aceña, J.; Pérez, S.; Barceló, D. Concentration and risk of pharmaceuticals in freshwater systems are related to the population density and the livestock units in Iberian Rivers. *Sci. Total Environ.* **2016**, *540*, 267–277. [CrossRef] [PubMed]

22. Castro, G.; Rodríguez, I.; Ramil, M.; Cela, R. Selective determination of sartan drugs in environmental water samples by mixedmode solid-phase extraction and liquid chromatography tandem mass spectrometry. *Chemosphere* **2019**, *224*, 562–571. [CrossRef]

23. Gurke, R.; Rößler, M.; Marx, C.; Diamond, S.; Schubert, S.; Oertel, R.; Fauler, J. Occurrence and removal of frequently prescribed pharmaceuticals and corresponding metabolites in wastewater of a sewage treatment plant. *Sci. Total Environ.* **2015**, *532*, 762–770. [CrossRef]

24. Ioannidi, A.; Arvaniti, O.S.; Nika, M.-C.; Aalizadeh, R.; Thomaidis, N.S.; Mantzavinos, D.; Frontistis, Z. Removal of drug losartan in environmental aquatic matrices by heat-activated persulfate: Kinetics, transformation products and synergistic effects. *Chemosphere* **2022**, *287*, 131952. [CrossRef]

25. Li, J.; Yang, L.; Lai, B.; Liu, C.; He, Y.; Yao, G.; Li, N. Recent progress on heterogeneous Fe-based materials induced persulfate activation for organics removal. *J. Chem. Eng.* **2021**, *414*, 128674. [CrossRef]

26. Chen, C.; Han, B.; Zhu, X.; Jiang, C.; Wang, Y. A novel pomegranate peel-derived biochar for highly efficient removal of sulfamethoxazole by activation of peroxymonosulfate through a non-radical pathway. *J. Environ. Chem. Eng.* **2022**, *10*, 108184. [CrossRef]

27. Tian, K.; Hu, L.; Li, L.; Zheng, Q.; Xin, Y.; Zhang, G. Recent advances in persulfate-based advanced oxidation processes for organic wastewater treatment. *Chin. Chem. Lett.* **2022**, *33*, 4461–4477. [CrossRef]

28. Ma, D.; Yi, H.; Lai, C.; Liu, X.; Huo, X.; An, Z.; Li, L.; Fu, Y.; Li, B.; Zhang, M.; et al. Critical review of advanced oxidation processes in organic wastewater treatment. *Chemosphere* **2021**, *275*, 130104. [CrossRef] [PubMed]

29. Chen, X.; Gudda, F.O.; Hu, X.; Waigi, M.G.; Gao, Y. Degradation of bisphenol A in an oxidation system constructed from Mo_2C MXene and peroxymonosulfate. *NPJ Clean Water* **2022**, *5*, 66. [CrossRef]

30. Guo, S.; Wang, H.; Yang, W.; Fida, H.; You, L.; Zhou, K. Scalable synthesis of Ca-doped α-Fe_2O_3 with abundant oxygen vacancies for enhanced degradation of organic pollutants through peroxymonosulfate activation. *Appl. Catal. B* **2020**, *262*, 118250. [CrossRef]

31. Ghanbari, F.; Moradi, M. Application of peroxymonosulfate and its activation methods for degradation of environmental organic pollutants: Review. *Chem. Eng. J.* **2017**, *310*, 41–62. [CrossRef]

32. Duan, R.; Ma, S.; Xu, S.; Wang, B.; He, M.; Li, G.; Fu, H.; Zhao, P. Soybean straw biochar activating peroxydisulfate to simultaneously eliminate tetracycline and tetracycline resistance bacteria: Insights on the mechanism. *Water Res.* **2022**, *218*, 118489. [CrossRef] [PubMed]

33. Tang, S.; Li, N.; Yuan, D.; Tang, J.; Li, X.; Zhang, C.; Rao, Y. Comparative study of persulfate oxidants promoted photocatalytic fuel cell performance: Simultaneous dye removal and electricity generation. *Chemosphere* **2019**, *234*, 658–667. [CrossRef] [PubMed]

34. Romanovski, V. Chapter 25—Agricultural waste based-nanomaterials: Green technology for water purification. In *Micro and Nano Technologies*; Abd-Elsalam, K.A., Zahid, M., Eds.; Aquananotechnology; Elsevier: Amsterdam, The Netherlands, 2021; pp. 577–595, ISBN 9780128211410. [CrossRef]

35. Ganesh, K.S.; Sridhar, A.; Vishali, S. Utilization of fruit and vegetable waste to produce value-added products: Conventional utilization and emerging opportunities—A review. *Chemosphere* **2022**, *287*, 132221. [CrossRef] [PubMed]

36. Zhang, A.; Li, X.; Xing, J.; Xu, G. Adsorption of potentially toxic elements in water by modified biochar: A review. *J. Environ. Chem. Eng.* **2020**, *8*, 104196. [CrossRef]

37. Cheng, N.; Wang, B.; Wu, P.; Lee, X.; Xing, Y.; Chen, M.; Gao, B. Adsorption of emerging contaminants from water and wastewater by modified biochar: A review. *Environ. Pollut.* **2021**, *273*, 116448. [CrossRef] [PubMed]

38. Kang, Z.; Jia, X.; Zhang, Y.; Kang, X.; Ge, M.; Liu, D.; Wang, C.; He, Z. A Review on Application of Biochar in the Removal of Pharmaceutical Pollutants through Adsorption and Persulfate-Based AOPs. *Sustainability* **2022**, *14*, 10128. [CrossRef]

39. Zhang, Y.; Liang, S.; He, R.; Zhao, J.; Lv, J.; Kang, W.; Zhang, J. Enhanced adsorption and degradation of antibiotics by doping corncob biochar/PMS with heteroatoms at different preparation temperatures: Mechanism, pathway, and relative contribution of reactive oxygen species. *J. Water Process. Eng.* **2022**, *46*, 102626. [CrossRef]

40. Wang, Y.; Song, Y.; Li, N.; Liu, W.; Yan, B.; Yu, Y.; Liang, L.; Chen, G.; Hou, L.; Wang, S. Tunable active sites on biogas digestate derived biochar for sulfanilamide degradation by peroxymonosulfate activation. *J. Hazard. Mater.* **2022**, *421*, 126794. [CrossRef] [PubMed]

41. Manikandan, S.; Vickram, S.; Subbaiya, R.; Karmegam, N.; Woong Chang, S.; Ravindran, B.; Kumar Awasthi, M. Comprehensive review on recent production trends and applications of biochar for greener environment. *Bioresour. Technol.* **2023**, *388*, 129725. [CrossRef]

42. Magangana, T.P.; Makunga, N.P.; Fawole, O.A.; Opara, U.L. Processing Factors Affecting the Phytochemical and Nutritional Properties of Pomegranate (*Punica granatum* L.) Peel Waste: A Review. *Molecules* **2020**, *25*, 4690. [CrossRef]

43. Siddiqui, M.T.H.; Nizamuddin, S.; Mubarak, N.M.; Shirin, K.; Aijaz, M.; Hussain, M.; Baloch, H.A. Characterization and Process Optimization of Biochar Produced Using Novel Biomass, Waste Pomegranate Peel: A Response Surface Methodology Approach. *Waste Biomass Valoriz.* **2019**, *10*, 521–532. [CrossRef]

44. Rouahna, N.; Salem, D.B.; Bouchareb, I.; Nouioua, A.; Ouakouak, A.; Fadel, A.; Hamdi, N.; Boopathy, R. Reduction of Crystal Violet Dye from Water by Pomegranate Peel–Derived Efficient Biochar: Influencing Factors and Adsorption Behaviour. *Water Air Soil Pollut.* **2023**, *234*, 324. [CrossRef]

45. Hadi, S.; Taheri, E.; Amin, M.M.; Fatehizadeh, A.; Khayet, M. Magnetized Activated Carbon Synthesized from Pomegranate Husk for Persulfate Activation and Degradation of 4-Chlorophenol from Wastewater. *Appl. Sci.* **2022**, *12*, 1611. [CrossRef]

46. Oymak, T.; Şafak, E.S. Removal of sulfadiazine from aqueous solution by magnetic biochar prepared with pomegranate peel. *Sep. Sci. Technol.* **2022**, *57*, 2521–2531. [CrossRef]

47. Taheri, E.; Fatehizadeh, A.; Lima, E.C.; Rezakazemi, M. High surface area acid-treated biochar from pomegranate husk for 2,4-dichlorophenol adsorption from aqueous solution. *Chemosphere* **2022**, *295*, 133850. [CrossRef] [PubMed]

48. Giannakopoulos, S.; Frontistis, Z.; Vakros, J.; Poulopoulos, S.G.; Manariotis, I.D.; Mantzavinos, D. Combined Activation of Persulfate by Biochars and Artificial Light for the Degradation of Sulfamethoxazole in Aqueous Matrices. *J. Taiwan Inst. Chem. Eng.* **2022**, *136*, 104440. [CrossRef]

49. Avramiotis, E.; Frontistis, Z.; Manariotis, I.D.; Vakros, J.; Mantzavinos, D. Oxidation of Sulfamethoxazole by Rice Husk Biochar-Activated Persulfate. *Catalysts* **2021**, *11*, 850. [CrossRef]

50. Dai, F.; Zai, J.; Yi, R.; Gordin, M.L.; Sohn, H.; Chen, S.; Wang, D. Bottom-up synthesis of high surface area mesoporous crystalline silicon and evaluation of its hydrogen evolution performance. *Nat. Commun.* **2014**, *5*, 3605. [CrossRef] [PubMed]

51. Fang, C.; Zhang, D. Pore forming with hemp fiber for magnesium phosphate structural supercapacitor. *Mater. Des.* **2020**, *186*, 108322. [CrossRef]

52. Waqas, M.; Aburiazaiza, A.S.; Miandad, R.; Rehan, M.; Barakat, M.A.; Nizami, A.S. Development of biochar as fuel and catalyst in energy recovery technologies. *J. Clean. Prod.* **2018**, *188*, 477–488. [CrossRef]

53. Gao, G.; Cheong, L.-Z.; Wang, D.; Shen, C. Pyrolytic carbon derived from spent coffee grounds as anode for sodium-ion batteries. *Carbon Resour. Convers.* **2018**, *1*, 104–108. [CrossRef]

54. Grilla, E.; Vakros, J.; Konstantinou, I.; Manariotis, I.D.; Mantzavinos, D. Activation of persulfate by biochar from spent malt rootlets for the degradation of trimethoprim in the presence of inorganic ions. *J. Chem. Technol. Biotechnol.* **2020**, *95*, 2348–2358. [CrossRef]

55. Kalampaliki, D.; Jayasinghe, G.D.T.M.; Avramiotis, E.; Manariotis, I.D.; Venieri, D.; Poulopoulos, S.G.; Szpunar, J.; Vakros, J.; Mantzavinos, D. Application of a KOH-activated biochar for the activation of persulfate and the degradation of sulfamethoxazole. *Chem. Eng. Res. Des.* **2023**, *194*, 306–317. [CrossRef]

56. Magioglou, E.; Frontistis, Z.; Vakros, J.; Manariotis, I.; Mantzavinos, D. Activation of Persulfate by Biochars from Valorized Olive Stones for the Degradation of Sulfamethoxazole. *Catalysts* **2019**, *9*, 419. [CrossRef]

57. Kaczmarczyk, B. FTIR study of conjugation in selected aromatic polyazomethines. *J. Mol. Struct.* **2013**, *1048*, 179–184. [CrossRef]

58. Bharath, G.; Latha, B.S.; Alsharaeh, E.H.; Prakash, P.; Ponpandian, N. Enhanced hydroxyapatite nanorods formation on graphene oxide nanocomposite as a potential candidate for protein adsorption, pH controlled release and an effective drug delivery platform for cancer therapy. *Anal. Methods* **2017**, *9*, 240–252. [CrossRef]

59. Giannakopoulos, S.; Vakros, J.; Frontistis, Z.; Manariotis, I.D.; Venieri, D.; Poulopoulos, S.G.; Mantzavinos, D. Biochar from Lemon Stalks: A Highly Active and Selective Carbocatalyst for the Oxidation of Sulfamethoxazole with Persulfate. *Catalysts* **2023**, *13*, 233. [CrossRef]

60. Ioannidi, A.; Frontistis, Z.; Mantzavinos, D. Destruction of propyl paraben by persulfate activated with UV-A light emitting diodes. *J. Environ. Chem. Eng.* **2018**, *6*, 2992–2997. [CrossRef]

61. Dimitrakopoulou, D.; Rethemiotaki, I.; Frontistis, Z.; Xekoukoulotakis, N.P.; Venieri, D.; Mantzavinos, D. Degradation, mineralization and antibiotic inactivation of amoxicillin by UV-A/TiO$_2$ photocatalysis. *J. Environ. Manag.* **2012**, *98*, 168–174. [CrossRef] [PubMed]

62. Ioannidi, A.A.; Arvaniti, O.S.; Miserli, K.; Konstantinou, I.; Frontistis, Z.; Mantzavinos, D. Removal of drug dexamethasone from aqueous matrices using low frequency ultrasound: Kinetics, transformation products, and effect of microplastics. *J. Environ. Manag.* **2023**, *328*, 117007. [CrossRef]

63. Frontistis, Z.; Mantzavinos, D. Sonodegradation of 17α-ethynylestradiol in environmentally relevant matrices: Laboratory-scale kinetic studies. *Ultrason. Sonochem.* **2012**, *19*, 77–84. [CrossRef]

64. Tosco, P.; Rolando, B.; Fruttero, R.; Henchoz, Y.; Martel, S.; Carrupt, P.-A.; Gasco, A. Physicochemical Profiling of Sartans: A Detailed Study of Ionization Constants and Distribution Coefficients. *HCA* **2008**, *91*, 468–482. [CrossRef]

65. Ioannidi, A.A.; Vlachodimitropoulou, M.; Frontistis, Z.; Petala, A.; Koutra, E.; Kornaros, M.; Mantzavinos, D. Assessing the Efficacy of a Mo$_2$C/Peroxydisulfate System for Tertiary Wastewater Treatment: A Study of Losartan Degradation, *E. coli* Inactivation, and Synergistic Effects. *Catalysts* **2023**, *13*, 1285. [CrossRef]

66. Shahzad, A.; Ali, J.; Ifthikar, J.; Aregay, G.G.; Zhu, J.; Chen, Z.; Chen, Z. Non-radical PMS activation by the nanohybrid material with periodic confinement of reduced graphene oxide (rGO) and Cu hydroxides. *J. Hazard. Mater.* **2020**, *392*, 122316. [CrossRef] [PubMed]

67. Ding, Y.; Wang, X.; Fu, L.; Peng, X.; Pan, C.; Mao, Q.; Wang, C.; Yan, J. Nonradicals induced degradation of organic pollutants by peroxydisulfate (PDS) and peroxymonosulfate (PMS): Recent advances and perspective. *Sci. Total Environ.* **2021**, *765*, 142794. [CrossRef] [PubMed]

68. De Andrade, J.R.; Vieira, M.G.A.; da Silva, M.G.C.; Wang, S. Oxidative degradation of pharmaceutical losartan potassium with N-doped hierarchical porous carbon and peroxymonosulfate. *J. Chem. Eng.* **2020**, *382*, 122971. [CrossRef]

69. Kemmou, L.; Frontistis, Z.; Vakros, J.; Manariotis, I.D.; Mantzavinos, D. Degradation of antibiotic sulfamethoxazole by biochar-activated persulfate: Factors affecting the activation and degradation processes. *Catal. Today* **2018**, *313*, 128–133. [CrossRef]

70. Wang, J.; Wang, C.; Guo, H.; Ye, T.; Liu, Y.; Cheng, X.; Li, W.; Yang, B.; Du, E. Crucial roles of oxygen and superoxide radical in bisulfite-activated persulfate oxidation of bisphenol AF: Mechanisms, kinetics and DFT studies. *J. Hazard. Mater.* **2020**, *391*, 122228. [CrossRef] [PubMed]

71. Zhu, S.; Li, X.; Kang, J.; Duan, X.; Wang, S. Persulfate Activation on Crystallographic Manganese Oxides: Mechanism of Singlet Oxygen Evolution for Nonradical Selective Degradation of Aqueous Contaminants. *Environ. Sci. Technol.* **2019**, *53*, 307–315. [CrossRef] [PubMed]

72. Lykoudi, A.; Frontistis, Z.; Vakros, J.; Manariotis, I.D.; Mantzavinos, D. Degradation of sulfamethoxazole with persulfate using spent coffee grounds biochar as activator. *J. Environ. Manag.* **2020**, *271*, 111022. [CrossRef]

73. Ho, S.-H.; Chen, Y.; Li, R.; Zhang, C.; Ge, Y.; Cao, G.; Ma, M.; Duan, X.; Wang, S.; Ren, N. N-doped graphitic biochars from C-phycocyanin extracted Spirulina residue for catalytic persulfate activation toward nonradical disinfection and organic oxidation. *Water Res.* **2019**, *159*, 77–86. [CrossRef]

74. Ntzoufra, P.; Vakros, J.; Frontistis, Z.; Tsatsos, S.; Kyriakou, G.; Kennou, S.; Manariotis, I.D.; Mantzavinos, D. Effect of sodium persulfate treatment on the physicochemical properties and catalytic activity of biochar prepared from spent malt rootlets. *J. Environ. Chem. Eng.* **2021**, *9*, 105071. [CrossRef]

75. Jawad, A.; Lang, J.; Liao, Z.; Khan, A.; Ifthikar, J.; Lv, Z.; Long, S.; Chen, Z.; Chen, Z. Activation of persulfate by CuOx@Co-LDH: A novel heterogeneous system for contaminant degradation with broad pH window and controlled leaching. *J. Chem. Eng.* **2018**, *335*, 548–559. [CrossRef]

76. Yang, L.; Chen, H.; Jia, F.; Peng, W.; Tian, X.; Xia, L.; Wu, X.; Song, S. Emerging Hexagonal Mo$_2$C Nanosheet with (002) Facet Exposure and Cu Incorporation for Peroxymonosulfate Activation Toward Antibiotic Degradation. *ACS Appl. Mater. Interfaces* **2021**, *13*, 14342–14354. [CrossRef]

77. Bao, Y.; Chen, T.; Zhu, Z.; Zhang, H.; Qiu, Y.; Yin, D. Mo$_2$C/C catalyst as efficient peroxymonosulfate activator for carbamazepine degradation. *Chemosphere* **2022**, *287*, 132047. [CrossRef]

78. Xu, L.; Wu, C.; Liu, P.; Bai, X.; Du, X.; Jin, P.; Yang, L.; Jin, X.; Shi, X.; Wang, Y. Peroxymonosulfate activation by nitrogen-doped biochar from sawdust for the efficient degradation of organic pollutants. *J. Chem. Eng.* **2020**, *387*, 124065. [CrossRef]

79. Zhou, H.; Lai, L.; Wan, Y.; He, Y.; Yao, G.; Lai, B. Molybdenum disulfide (MoS$_2$): A versatile activator of both peroxymonosulfate and persulfate for the degradation of carbamazepine. *J. Chem. Eng.* **2020**, *384*, 123264. [CrossRef]

80. Kohantorabi, M.; Moussavi, G.; Giannakis, S. A review of the innovations in metal- and carbon-based catalysts explored for heterogeneous peroxymonosulfate (PMS) activation, with focus on radical vs. non-radical degradation pathways of organic contaminants. *J. Chem. Eng.* **2021**, *411*, 127957. [CrossRef]

81. Ntaflou, M.; Vakros, J. Transesterification activity of modified biochars from spent malt rootlets using triacetin. *J. Clean. Prod.* **2020**, *259*, 120931. [CrossRef]

82. Zeng, M.; Shah, S.A.; Huang, D.; Parviz, D.; Yu, Y.-H.; Wang, X.; Green, M.J.; Cheng, Z. Aqueous Exfoliation of Graphite into Graphene Assisted by Sulfonyl Graphene Quantum Dots for Photonic Crystal Applications. *ACS Appl. Mater. Interfaces* **2017**, *9*, 30797–30804. [CrossRef] [PubMed]

83. Luo, J.; Zeng, M.; Peng, B.; Tang, Y.; Zhang, L.; Wang, P.; He, L.; Huang, D.; Wang, L.; Wang, X.; et al. Electrostatic-Driven Dynamic Jamming of 2D Nanoparticles at Interfaces for Controlled Molecular Diffusion. *Angew. Chem. Int. Ed.* **2018**, *57*, 11752–11757. [CrossRef] [PubMed]

84. Potakis, N.; Frontistis, Z.; Antonopoulou, M.; Konstantinou, I.; Mantzavinos, D. Oxidation of bisphenol A in water by heat-activated persulfate. *J. Environ. Manag.* **2017**, *195*, 125–132. [CrossRef] [PubMed]

85. Dhoke, S.K. Determination of alkalinity in the water sample: A theoretical approach. *Chem. Teach. Int.* **2023**, *5*, 283–290. [CrossRef]

86. Giannakopoulos, S.; Vakros, J.; Dracopoulos, V.; Manariotis, I.D.; Mantzavinos, D.; Lianos, P. Enhancement of the photoelectrocatalytic degradation rate of a pollutant in the presence of a supercapacitor. *J. Clean. Prod.* **2022**, *377*, 134456. [CrossRef]

87. Avramiotis, E.; Frontistis, Z.; Manariotis, I.D.; Vakros, J.; Mantzavinos, D. On the Performance of a Sustainable Rice Husk Biochar for the Activation of Persulfate and the Degradation of Antibiotics. *Catalysts* **2021**, *11*, 1303. [CrossRef]

88. Kayode, C.A. Chapter 8—Residence Time Distributions in Flow Reactors. In *Modeling of Chemical Kinetics and Reactor Design*; Elsevier: Amsterdam, The Netherlands, 2001; pp. 663–761. [CrossRef]